Journal of Applied Polymer Science

# Influence of nanovermiculites with a high aspect ratio and stretch orientation on the microstructure of polypropylene films

**Wen Cai Xu, Dong Li Li, Ya Bo Fu, Rui Juan Liao, Jia Zi Shi, Ya Jun Wang, Xiao Hui He**
Beijing Key Laboratory of Printing and Packaging Materials and Technology, Beijing Institute of Graphic Communication, Beijing 102600, People's Republic of China
Correspondence to: D. L. Li (E-mail: lidongli6666@126.com)

**ABSTRACT:** In this article, we present a process for preparing organovermiculites, which consist of expanded vermiculite (EVMT)–poly(vinyl alcohol) (PVOH) created by the mechanical ball-milling of EVMT in a PVOH–water solution. We then discusses the influence of EVMT–PVOH on the barrier performance, crystallization behavior, thermal stability, and mechanical properties of modified blown polypropylene (PP) films. EVMT was intercalated and exfoliated by PVOH macromolecules to obtain a kind of hybrid EVMT–PVOH. PVOH served as both an intercalating agent into EVMT and a compatibilizer between EVMT and PP. Compared with the original (unmodified) PP, when the EVMT loading ranged from 0.1 to 2.0%, although the crystallinity decreased for most PP films, the thermal stability and mechanical properties all improved. Moreover, EVMT platelike particles with a high aspect ratio (ca. 550) dispersed in the PP matrix also improved the barrier properties of the modified PP films, which was in accordance with the Nielsen model. © 2015 Wiley Periodicals, Inc. J. Appl. Polym. Sci. **2016**, *133*, 42846.

**KEYWORDS:** blends; differential scanning calorimetry (DSC); films; packaging; thermogravimetric analysis (TGA)

Received 20 March 2015; accepted 14 August 2015
**DOI: 10.1002/app.42846**

## INTRODUCTION

Vermiculite (VMT) is a mica-type phyllosilicate composed of a tetrahedral–octahedral–tetrahedral layer and an interlayer (gallery) containing $Mg^{2+}$ hydration cations and minor amounts of $Ca^{2+}$, $Na^{+}$, and $K^{+}$.[1] As set forth in the literature, organovermiculite (organo-VMT) can be prepared with the ion-exchange method, with $H^{+}$,[2] alkyl ammonium salt,[3,4] or maleic anhydride.[5,6] However, the organo-VMTs prepared in these experiments have been unsuitable for food-packaging materials because alkyl ammonium salt and maleic anhydride both have a degree of toxicity. In our previous studies, we used ethylene–vinyl acetate copolymer (EVA) as an intercalating agent into expanded vermiculite (EVMT).[7,8] Although the EVMT–EVA combination greatly improved the mechanical properties of polypropylene (PP) films, they made less of a contribution to the barrier properties because the aspect ratio of the platelike particles in EVMT–EVA was less than 50.

In this article, we present a new process for the preparation of organo–EVMT through the ball-milling of EVMT in a poly(vinylalcohol) (PVOH) aqueous solution to exfoliate EVMT to nano-size. We examined the effects of the new process on the crystallization behavior, thermal stability, and mechanical properties of the PP films modified by the EVMT–PVOH combination. The X-ray diffraction (XRD) analysis results show that the PVOH macromolecules served well as intercalating agents into the interlayers of EVMT; this caused exfoliation or separation of the layers of the EVMT host structure. The platelike nanoparticles in EVMT–PVOH had a high aspect ratio (ca. 550) in PP, as confirmed by the Nielsen model. The PVOH macromolecules served well as compatibilizers between the platelike nanoparticles and the PP matrix in the PP–EVMT–PVOH melt blend because no interface separated them, as we observed in the scanning electron microscopy (SEM) analysis.

After the modified PP films were prepared from the PP–EVMT–PVOH nanocomposites, their crystallization behavior, mechanical properties, and thermal stability were measured. Compared with the original (nonmodified) PP, when the EVMT–PVOH loading ranged from 0.1 to 2.0%, although the crystallinity decreased by 7–38% and the elongation at break decreased gradually, the tensile strength increased by 4–12%. Furthermore, Young's modulus increased by 4–14%, the stress at break increased by 28–158%, the thermal stability increased by 10.9–24.9°C, and the barrier properties increased by 5.4–93.6%. In comparison with the traditional process for preparing organo-VMT, the new process for preparing EVMT–PVOH described in this article was simple, safe, and suitable for food packaging.

## EXPERIMENTAL

### Materials

The VMT used in this experiment was EVMT from the Yuli (Weili) Co. Qeganbulak VMT deposit in Xinjiang, China. The EVMT was obtained by the treatment of the natural VMT by quickly going through the channel-type furnace at 1100°C. PVOH resin with Elvanol grade 90–50 was purchased from DuPont (Pudong New District, Shanghai, China). PP was purchased from MaoMing SINOPEC (MaoMing, China) with grade F280 (PPH-F-022-A); it was a special PP homopolymer for PP with a melt flow index of 2.8 g/10 min and an isotacticity of 96.5%.

### Preparation of EVMT–PVOH

A certain mass of PVOH was added to water that was heated gently until the PVOH dissolved. The EVMT was crushed in a high-speed pulverizer for 5 min, sieved to get 50–100-mesh EVMT, and mixed with the prepared PVOH–water solution. The mixture was ball-milled at a speed of 2000 rpm in a high-speed ball miller (GJ-28, Qingdao Haitong Special Instrument Co., Ltd., Qingdao City, China) for 30 min. Then, EVMT–PVOH slurry was dried in an oven at 70°C for 24 h in a vacuum. The final pellet-form EVMT–PVOH (5:95 wt %) was obtained by cutting and was characterized with XRD.

### Preparation of the EVMT–PVOH–PP Nanocomposite Blends

The EVMT–PVOH–PP polymer–matrix composites (nanocomposites) were prepared in a screw extruder [CTE-35, Coperion Keya (Nanjing) Machinery Co., Ltd., China] at 300 rpm. The melt-blending temperature profiles selected were 185, 200, 215, and 230°C. The weight ratios (weight percentage) of EVMT–PVOH to PP were fixed at 0.1, 0.3, 0.5, 1.0, 1.5, and 2.0. The EVMT–PVOH–PP nanocomposites were pelletized and dried at 60°C for 3 h. The weight ratios of PP to EVMT to PVOH in the polymer–matrix composite samples 1–7 were 100:0:0, 99.8:0.1:0.1, 99.4:0.3:0.3, 99.0:0.5:0.5, 98.0:1.0:1.0, 97.0:1.5:1.5, and 96.0:2.0:2.0, respectively.

### Preparation of Films

The EVMT–PVOH–PP blend films were prepared with a blown-film extruder (Laiwu Jingrui Plastic Machinery Co., Ltd., Shangdong, China) at extruder temperatures of four states: 170, 190, 210, and 230°C. The thickness of the film was 25 $\mu$m. The films were characterized with thermogravimetric analysis (TGA), Fourier transform infrared (FTIR) spectroscopy, differential scanning calorimetry (DSC), and SEM.

### Analysis Methods

**XRD Analysis.** XRD patterns were carried out in a D/max2550HB+/PC X-ray diffractometer (Rigaku, Japan) with a graphite monochromator and a Cu K$\alpha$ radiation source ($\lambda = 0.154439$ nm) operated at 40 kV/200 mA. The diffraction patterns were collected within the $2\theta$ range 1.5–50° with a step of 0.02° and a scanning rate of 4 s.

**Analysis of the Mechanical Properties.** The mechanical properties, such as the tensile strength, modulus of elasticity (Young's modulus), elongation at break, and breaking stress, of PP were tested with a 5565A Instron universal testing machine (Norwood, MA) at a crosshead speed of 50 mm/min according to ASTM D 638.

**SEM Analysis.** The morphology of the fracture cross section of PP dumbbell specimens was performed with an SS-550 SEM (Shimadzu, Japan) at an accelerating voltage of 10 kV. The brittle fracture cross section of the PP films was prepared according to the following method. The PP films were immersed in liquid nitrogen for 2 min. We then removed them from the liquid nitrogen and quickly sheared them off with a scissors. We took the fractured surfaces to prepare cross sections and then performed gold sputtering and testing.

**DSC Analysis.** We determined the crystallization onset temperature, peak temperature, and end temperatures and the enthalpy of crystallization ($\Delta H_c$) of PP films with Netzsch DSC-200PC instrument (Selb, Germany). The instrument was calibrated with indium as a standard. We prepared the samples by sealing them in aluminum pans with a mass of 5–10-mg weights, and all of the experiments were performed under a nitrogen gas flow. The samples were heated from −25 to 210°C at 20°C/min, held for 5 min to erase any thermal history, cooled to 55°C at 10°C/min, held for 5 min, subsequently heated to 210°C at 20°C/min, and held for 5 min. The degree of crystallinity of each specimen was calculated with the melting enthalpy of 100% crystalline PP considered to be 165 J/g.[9]

**Barrier Analysis.** The oxygen transmission rates (OTRs) of the PP films were obtained with a Systech Illinois 8001 oxygen permeation analyzer (Johnsburg, IL) at 30°C and 1 atm.

**FTIR Analysis.** The IR spectrometry of the PP films was performed with an FTIR-8400 apparatus (Shimadzu, Japan) equipped with the IR solution and 32-bit high-performance FTIR software.

**Thermal Analysis.** Thermogravimetry was conducted with a Netzsch TG-209 thermogravimetric analyzer. Samples were weighed into standard aluminum pans. A sealed empty pan was used as a reference while nitrogen gas was purged at 20 mL/min during the experiments. Initially, each sample was heated to 25°C, and scanning was carried out at temperatures ranging from 25 to 500°C at 20°C/min.

**Statistical Analysis.** The mechanical properties of each PP film were measured seven times; this was followed by averaging and variance analysis with a confidence level of less than 0.05 (except for the stress at break and elongation at break).

## RESULTS AND DISCUSSION

### PVOH Intercalation into EVMT

Natural VMT is a mica-type silicate with a 2:1 layered phyllosilicate, and the basal spacing ($d_{001}$) of its structural unit is about 1.4 nm, depending on the water interlamellar layers and the interlayer cations.[10] Some small molecules can be exchanged with interlayer cations and can, thereby, increase $d_{001}$. Macromolecules with random coil conformations are difficult to get through the narrow interlayer, but macromolecules are able to smoothly enter into the interlayer of EVMT because the interlayer space of EVMT is much larger than that of natural, unexpanded VMT. Heating VMT rapidly to 1100°C results in the

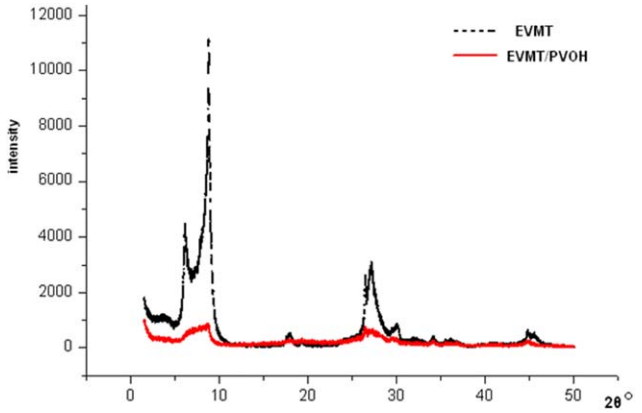


**Figure 1.** XRD patterns of EVMT and EVMT–PVOH. [Color figure can be viewed in the online issue, which is available at wileyonlinelibrary.com.]

transformation of the interlayer water into steam, and great thermal expansion of the VMT after the explosive dehydration of the interlayer water causes cracking of the VMT platelets,[11] increasing lattice defects, twist distortion of the platelets, and decreasing orderliness of the *c* axis of EVMT.[12]

Figure 1 and Table I show that the Yuli EVMT exhibited characteristic diffraction peaks at 2$\theta$s of 6.09, 17.77, and 29.88°; these belonged to the respective crystal planes (001), (003), and (005) of EVMT. Other characteristic diffraction peaks of the crystal plane, such as (002) and (004), were not observed because there were lattice defects and twist distortions of platelets in the EVMT. The characteristic diffraction peaks at 2$\theta$s of 8.77 and 26.45°, which belonged to the crystal plane (001) and (003), respectively, of mica, showed that the Yuli EVMT consisted of mixed-layer VMT–mica (phlogopite) at a ratio of 1:1.[13–15] As a result of the ball-milling shear effect, the PVOH macromolecules entered into the interlayer space of EVMT, separated the platelets, and increased the $d_{001}$ of EVMT; this resulted in the shift of the (001) characteristic diffraction peaks to small angles in the XRD spectra. In the range of 2$\theta$s between 1.50 and 6.09°, the characteristic diffraction peak of $d_{001}$ (001) of the intercalated EVMT was not observed. This showed that $d_{001}$ was greater than 5.899 nm, and the PVOH was intercalated into EVMT successfully. This increased $d_{001}$ was greater than that for the other molecules, such as alkyl ammonium salt or maleic anhydride, intercalating in EVMT.

The intercalation of PVOH into EVMT was confirmed not only by XRD but also by FTIR analysis. Figure 2 and Table II represent the important characteristic peaks of EVMT, PVOH, and

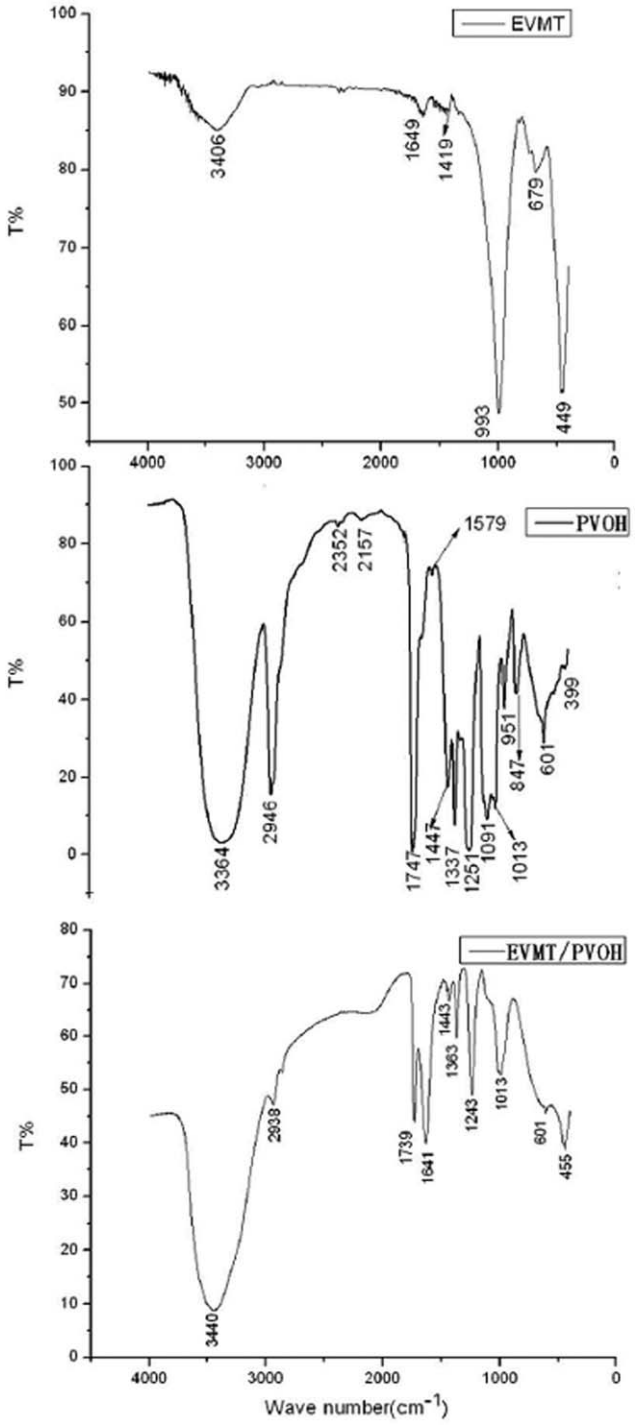


**Figure 2.** FTIR spectra of PVOH, EVMT, and EVTM–PVOH.

**Table I.** Positions of the Diffraction Peaks of the Pure EVMT and EVMT–PVOH

| | | VMT (001) | Mica (001) | VMT (002) | VMT (003) | VMT (004) | Mica (003) | Impurity | VMT (005) |
|---|---|---|---|---|---|---|---|---|---|
| EVMT | 2$\theta$ (°) | 6.09 | 8.77 | — | 17.77 | — | 26.45 | 27.13 | 29.88 |
| | *d* (nm) | 1.454 | 1.010 | — | 0.4972 | — | 0.3375 | 0.3292 | 0.2995 |
| EVMT–PVOH | 2$\theta$ (°) | — | 8.75 | — | 17.87 | — | 26.45 | — | — |
| | *d* (nm) | — | 1.010 | — | 0.4972 | — | 0.3375 | — | — |

*d*, lattice plane spacing.

**Table II.** Characteristic FTIR Peaks for PVOH, EVMT, and EVTM–PVOH

| Bond | Wave number in PVOH ($cm^{-1}$) | Wave number in EVMT ($cm^{-1}$) | Wave number in EVMT–PVOH ($cm^{-1}$) |
|---|---|---|---|
| O—H stretching | 3364 | 3406 | 3440 |
| C—H stretching | 2946 | — | 2938 |
| Residual acetate groups | 1747 | — | 1739 |
| O—H bending | — | — | 1641 |
| C—O stretching in C—O—H | 1091 | — | 1013 |
| Si—O stretching | — | 993 | — |
| C—O stretching in C—O—C | 1013 | — | 1013 |

EVMT–PVOH with a weight ratio of EVMT to PVOH of 5:95, respectively. As shown in Figure 2, their hydroxyl (—OH) characteristic stretching peak occurred at 3364, 3406, and 3440 $cm^{-1}$ in PVOH, EVMT, and EVMT–PVOH, respectively. The O—H characteristic stretching peak appeared at higher wave numbers in EVMT than in PVOH. This was due to the high bond energy of OH in EVMT; thus, the stretching vibration absorption of —OH of EVMT was higher because a higher wave number denoted the extra energy required to convert into kinetic energy and to induce a vibration effect in the EVMT hydroxyl group. Unusually, the O—H characteristic stretching peaks from the Si—OH at 3406 $cm^{-1}$ for the EVMT shifted to a higher wave number (3440 $cm^{-1}$) for EVMT–PVOH. This shift of the peak to higher wave numbers was consistent with findings of previous literature,[16] most probably because of the strong interactions of PVOH–EVMT in this nanocomposite.

Another important peak was found at a wave number of 1641 $cm^{-1}$, which represented the bending vibrational absorption of the hydroxyl group[17] for PVOH in EVMT–PVOH; however, the bending vibrational absorption was not found in the pure PVOH because PVOH in EVMT–PVOH had a higher crystallinity compared with pure PVOH. In fact, PVOH was produced from the input of poly(vinyl acetate), where imperfect hydrolysis caused trace vinyl acetate to remain in PVOH. The remaining vinyl acetate groups disrupted the main-chain regularity, decreasing the crystallizing ability of PVOH to crystallize. By contrast, in the EVMT–PVOH nanocomposites, the —OH in EVMT strongly attracted PVOH macromolecules; this resulted in PVOH's regular arrangement on the EVMT surface, an increase in the PVOH crystallinity, and the formation of a microstructure of EVMT nanoparticles packaged with PVOH.

### Affinity of EVMT–PVOH to PP

PVOH consists of polar macromolecules whose chains contain many hydroxyl groups. It is highly compatible with EVMT because its hydroxyl groups form complex structures with interlayer ions, such as $K^+$, $Mg^{2+}$, and $Ca^{2+}$, in EVMT. PVOH macromolecules are adsorbed around pallets of EVMT and well-packaged nano-EVMT particles. PVOH exerts some compatibility with the PP matrix,[18] it has been proven in other preparations of biaxially oriented PP–PVOH films[19] and PP–PVOH fibers,[20] and of course, It is better to use some compatibilizer in any case.

In this research, PVOH's compatibility with EVMT and PP was found to be beneficial for the dispersion of EVMT platelets into the PP matrix under shear force and stretching effects during the film-blowing process. All of the SEM images of the brittle fractures of the PP–EVMT–PVOH films are shown in Figure 3. They were not found to cause agglomeration or edges around the VMT pallets, holes, or any separate surface because of the detachment of VMT from the PP matrix; this indicated that PP and PVOH closely packaged EVMT pallets. Instead, EVMT produced an entirely different morphology in the PP–EVMT–PVOH blended films. Without EVMT, the micrograph of the pure PP film (sample 1, named PP-0.0%) and modified PP with low EVMT concentration (sample2 with 0.1% EVMT, named PP-0.1%) exhibited smooth, brittle cross-surface fractures. However, samples 3–6 with 0.3–1.5% EVMT exhibited elongated fibrils extending over the surface; this indicated that EVMT improved the toughness of PP. EVMT was also found to increase the brittleness when its concentration was greater than 2.0%, and sample 7 exhibited smooth, brittle cross-surface fractures. These findings show that EVMT exfoliated and dispersed within the PP matrix by melt-blending, whereas the PP chain intercalated into the EVMT galleries, and the EVMT layers underwent exfoliation under shearing force.

### Effect of EVMT on the Crystallization Behavior of Modified PP Films

Polar EVMT had a large particle surface and strongly interacted with the surrounding PVOH macromolecules chains. The PP macromolecule chains interacted with EVMT by means of PVOH as a compatibilizer. In the composites, the physical interactions between PP and EVMT–PVOH played an important role in improving the compatibility, as monitored by DSC analysis. Figure 4 shows the DSC curves of PP-0.1% and contains the first heating curve (with the thermal history), cooling curve, and second heating curve.

Table III shows the cooling crystallization onset temperature ($T_C^{on}$), cooling crystallization peak temperature ($T_C^p$), and cooling crystallization end temperature ($T_C^e$) for all of the modified PP (EVMT–PVOH–PP) films after the removal of the previous thermal history. Under nonisothermal cooling conditions, compared with the original PP (PP-0.0%), $T_C^{on}$, $T_C^p$, and $T_C^e$ of sample PP-0.1% shifted to higher temperatures. This implied that the EVMT played a part in heterogeneous nucleation and increased the PP crystallization rates at higher temperatures.

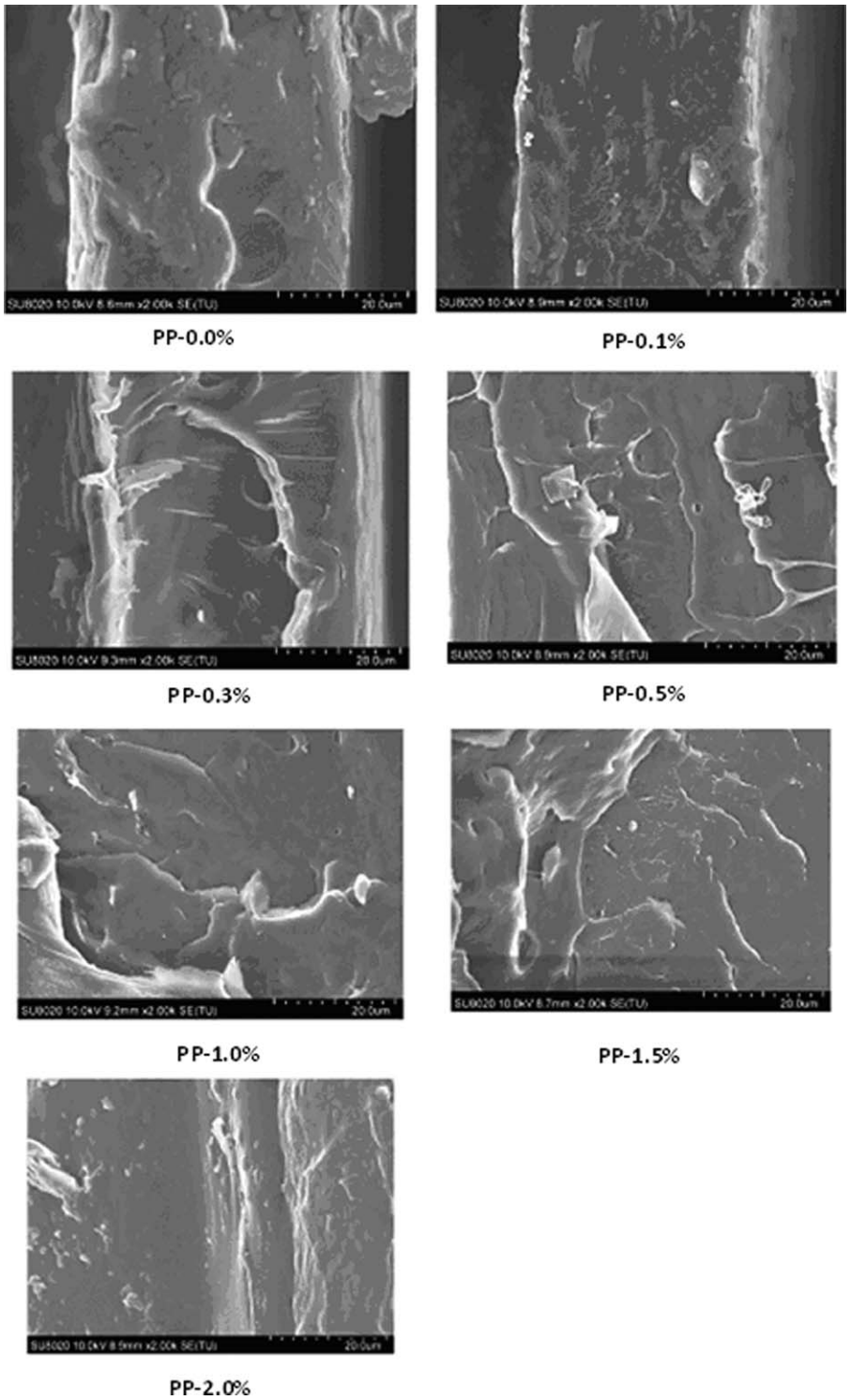


**Figure 3.** Micrographs of the brittle tensile surfaces of PP–EVMT–PVOH blended films at 2000× magnification.

The $T_C^{on}$, $T_C^p$, and $T_C^e$ values of the other samples displayed a similar phenomenon; namely, all of the $T_C^{on}$ and $T_C^e$ values increased. The width of the crystallization peak ($\Delta T = T_C^{on} - T_C^e$) was directly related to the crystallization rate; that is, a smaller $\Delta T$ value meant that the crystallization rate value was bigger, and the crystallization process was faster. Compared with the original sample 0, all of the $\Delta T$ values of samples 2–6 showed a decrease; this demonstrated that the EVMT platelike particles accelerated the crystallization process. Although the original crystallinity data did not show an obvious influence of EVMT on the PP crystallinity, the adjusted $\Delta H_c$ demonstrated that the EVMT platelike particles increased the crystallinity of the modified PP films, except in sample 3 (PP-0.3%), after EVMT and PVOH were deducted from the PP film samples,

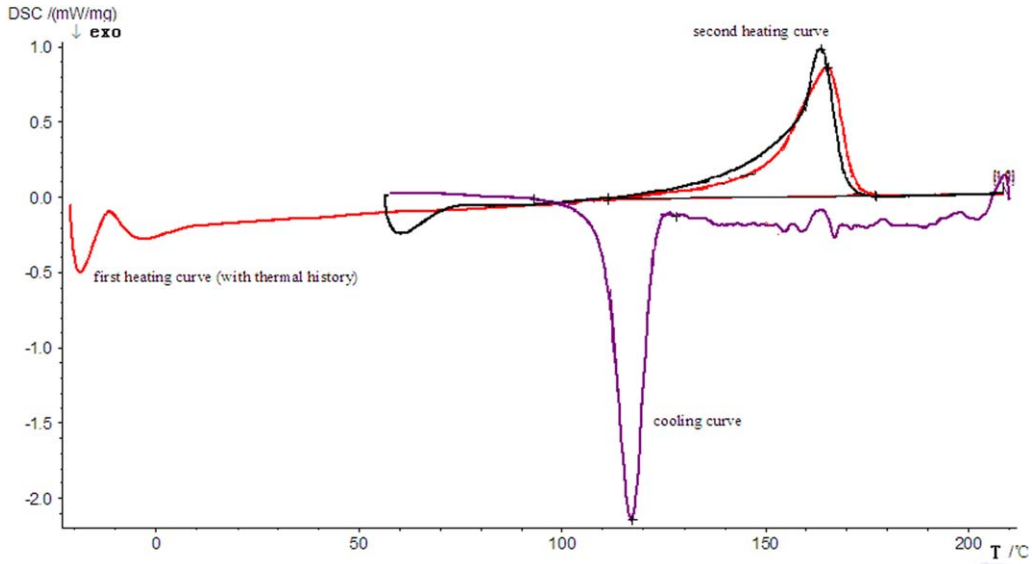


**Figure 4.** DSC curves of PP-0.1% (T=temperature). [Color figure can be viewed in the online issue, which is available at wileyonlinelibrary.com.]

because EVMT and PVOH made no contribution to $\Delta H_c$. For sample 6, more EVMT slowed the PP macromolecules' rate of movement and impeded the PP crystallization process.[21,22]

The DSC analysis of the melting temperature for the PP films (before the removal of the previous thermal history) isolated the effect of the EVMT platelike particles and stretch orientation (film-blowing process) on the crystallization behavior (Table IV).

The stretch orientation in the film-blowing process made the EVMT platelike particles move in relation to one another and arranged themselves in a parallel fashion. Many PP chains were driven by movement caused by the dislocation and slipping of platelike particles, and these chains were connected by van der Waals forces. This behavior was beneficial to inducing PP chain–oriented crystallization, as confirmed by the DSC data of the PP films with a previous thermal history. As shown in Table IV, compared with sample 1 (pure PP without filling EVMT), the melting onset temperature ($T_m^{on}$), melting peak temperature ($T_m^p$), and melting end temperature ($T_m^e$) all rose with increasing nanoparticle content. These data display the increasing thermostability of the PP films with platelike nanoparticles.

From second-heating DSC data of the PP films with the previous thermal history removed (Table V), the $T_m^{on}$ and crystallinity for the annealed PP films with filling platelike particles were lower than those without annealing. This proved that the stretching orientation enhanced the effect of the platelike particles on oriented crystallization in the film-blowing process. In the film-blowing process, the time from the extrusion die to the cooling roller was short, shorter than the PP chain relaxation time, and this could cause defects in the crystal. Theoretically, these crystal defects will be recovered after the removal of any previous thermal history that increased crystallinity, and the volume $T_m^{on}$ and $T_m^p$ for annealed PP films with perfect crystal formation were higher than they were without annealing; however, the reality was contrasted because of the stretch orientation of the PP chains and EVMT platelike particles in the preparation of our modified PP film.

### Effect of EVMT on the Thermal Stability of Modified PP Films

The thermal properties of the PP films with or without EVMT filling were determined by TGA (Figure 5) and are summarized in Table VI. Table VI lists the onset temperature of degradation ($T_{de}^{on}$), as measured by the temperatures at which 5, 10, and 50% of mass were lost ($T_{5\%}$, $T_{10\%}$, and $T_{50\%}$, respectively).

As shown in Figure 4, for EVMT, no weight loss was observed at 25–500°C. Pure PVOH started to decompose at 170.2°C, but

**Table III.** DSC Data for the PP Films Obtained from the Cooling DSC Runs (after the Removal of the Previous Thermal History)

| PP sample | EVMT (%) | PVOH (%) | $\Delta H_c$ (J/g) | Adjusted $\Delta H_c$ (J/g) | $T_C^{on}$ (°C) | $T_C^p$ (°C) | $T_C^e$ (°C) | $T_C^{on} - T_C^e$ (°C) |
|---|---|---|---|---|---|---|---|---|
| 1 | 0 | 0 | −88.7 | −88.7 | 119.9 | 116.7 | 105.4 | 14.5 |
| 2 | 0.1 | 0.1 | −90.0 | −90.2 | 122.6 | 117.1 | 110.4 | 12.2 |
| 3 | 0.3 | 0.3 | −81.7 | −82.2 | 121.4 | 115.1 | 107.2 | 14.2 |
| 4 | 0.5 | 0.5 | −87.7 | −88.6 | 120.7 | 115.3 | 108.2 | 12.5 |
| 5 | 1.0 | 1.0 | −87.2 | −89.0 | 120.3 | 114.6 | 107.1 | 13.2 |
| 6 | 1.5 | 1.5 | −86.6 | −89.3 | 120.0 | 114.1 | 105.7 | 14.3 |
| 7 | 2.0 | 2.0 | −83.2 | −86.7 | 119.9 | 113.9 | 106.5 | 13.1 |

**Table IV.** DSC Data for the PP Films Obtained from the First-Heating DSC Runs (with the Previous Thermal History)

| PP sample | EVMT (%) | PVOH (%) | $\Delta H_m$ (J/g) | Adjusted $\Delta H_m$ (J/g) | $T_m^{on}$ (°C) | $T_m^{p}$ (°C) | $T_m^{e}$ (°C) |
|---|---|---|---|---|---|---|---|
| 1 | 0 | 0 | 88.5 | 88.5 | 149.0 | 159.7 | 168.2 |
| 2 | 0.1 | 0.1 | 90.4 | 90.6 | 157.4 | 163.6 | 169.7 |
| 3 | 0.3 | 0.3 | 78.9 | 79.4 | 156.5 | 163.1 | 170.8 |
| 4 | 0.5 | 0.5 | 79.6 | 80.4 | 156.3 | 164.3 | 171.3 |
| 5 | 1.0 | 1.0 | 74.0 | 75.5 | 157.1 | 164.8 | 171.7 |
| 6 | 1.5 | 1.5 | 64.4 | 66.4 | 157.7 | 165.9 | 173.1 |
| 7 | 2.0 | 2.0 | 60.1 | 62.6 | 158.0 | 164.8 | 171.5 |

$\Delta H_m$, melting enthalpy

**Table V.** DSC Data for the PP Films Obtained from the Second-Heating DSC Runs (after the Removal of the Previous Thermal History)

| PP sample | EVMT (%) | $\Delta H_m$ (J/g) | Adjusted $\Delta H_m$ (J/g) | $T_m^{on}$ (°C) | $T_m^{p}$ (°C) | $T_m^{e}$ (°C) |
|---|---|---|---|---|---|---|
| 1 | 0 | 82.4 | 82.4 | 149.0 | 159.7 | 170.2 |
| 2 | 0.1 | 84.2 | 84.4 | 150.5 | 165.5 | 171.5 |
| 3 | 0.3 | 72.7 | 73.1 | 150.6 | 164.8 | 171.7 |
| 4 | 0.5 | 74.7 | 75.5 | 152.5 | 164.9 | 172.9 |
| 5 | 1.0 | 70.8 | 72.2 | 153.1 | 165.5 | 172.5 |
| 6 | 1.5 | 64.8 | 66.8 | 153.6 | 165.9 | 173.4 |
| 7 | 2.0 | 60.0 | 62.5 | 153.8 | 165.8 | 173.0 |

$\Delta H_m$, melting enthalpy

EVMT–PVOH (5:95 wt %) was stable before 258.5°C; this showed that strong intermolecular forces, for example, hydrogen bonds, were formed between EVMT and PVOH, so the thermal decomposition temperature of EVMT–PVOH was higher than that of pure PVOH. All of the thermal degradation profiles of the modified PP films exhibited two main stages: one starting at 260–305°C (first stage) and another starting at 360–450°C (second stage). In the first stage, $T_{de}^{on}$ of the pure PP film started at 276.6°C. $T_{de}^{on}$ of PP with EVMT filling was higher than that of the pure PP film (except for PP films 3 and 4). The values of $T_{5\%}$, $T_{10\%}$, and $T_{50\%}$ were also higher for PP with EVMT filling than for the pure PP film, with the exception of PP film 4.

The EVMT platelike particles exerted two effects on the thermal degradation profiles: one was heterogeneous nucleation, which contributed to the improvement of the thermal stability, and the other was an increase in the melt viscosity, which resulted in the slow movement of PP chain segments and increasing crystal defects, which in turn, led to a decreasing thermal stability. These two effects of EVMT changed according to different filling amounts of EVMT. For example, $T_{de}^{on}$ of PP-1.0% showed a 20.6°C higher thermal resistance than the pure PP. Also, the values of $T_{5\%}$, $T_{10\%}$, and $T_{50\%}$ of PP-1.0% showed 20.6, 31.5, and 35.3°C higher thermal resistances, respectively, than those of pure PP. For PVOH, $T_{de}^{on}$ was 170.2°C, and its maximum weight loss temperature range was 297–324°C. On the basis of the TGA curves shown in Figure 4, a $T_{de}^{on}$ of about 170°C for the PP films with EVMT–PVOH was obvious. This showed that EVMT within the interlayer cations interacted with PVOH and formed an EVMT–PVOH complex; this resulted in the disappearance of the properties of PVOH alone. This also agreed with the previous FTIR analysis.

As shown from the previous analysis of the degradation temperature of pure PP, PP with EVMT–PVOH, and pure PVOH, the increasing thermal stability of PP with EVMT–PVOH was caused by the filling of the platelike particles of EVMT, which acted as a heat barrier. These enhanced the overall thermal stability of the PP–EVMT–PVOH composites and assisted in the formation of char during thermal degradation.[2,23]

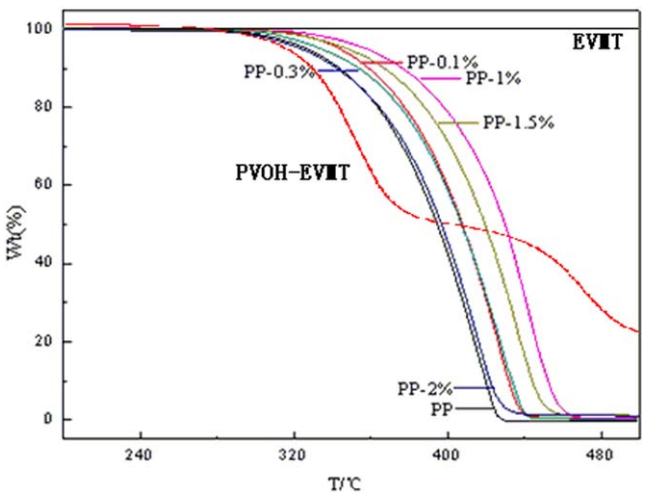


**Figure 5.** Thermogravimetric curves for PP films with and without EVMT filling (T=temperature). [Color figure can be viewed in the online issue, which is available at wileyonlinelibrary.com.]

**Table VI.** TGA Data for the PP Films with and without EVMT Filling

| PP sample | EVMT (%) | $T_{de}^{on}$ (°C) | $T_{5\%}$ (°C) | $T_{10\%}$ (°C) | $T_{50\%}$ (°C) |
|---|---|---|---|---|---|
| EVMT | 100.0 | — | — | — | — |
| Pure PVOH | 0.0 | 170.2 | 260.4 | 295.4 | 348.1 |
| PVOH-EVMT | 5.0 | 258.5 | 300.4 | 327.1 | 400.5 |
| 1 | 0.0 | 276.6 | 326.1 | 343.6 | 394.8 |
| 2 | 0.1 | 288.6 | 343.9 | 358.9 | 407.8 |
| 3 | 0.3 | 267.5 | 333.6 | 353.7 | 407.5 |
| 4 | 0.5 | 262.0 | 303.0 | 319.2 | 371.0 |
| 5 | 1.0 | 297.2 | 357.6 | 375.1 | 430.1 |
| 6 | 1.5 | 301.5 | 347.6 | 366.7 | 419.5 |
| 7 | 2.0 | 287.5 | 323.6 | 342.4 | 397.0 |

### Effect of EVMT on the Mechanical Properties of the Modified PP Films

The mechanical properties of the polymeric materials are well known to be related to their morphology, such as the crystallinity and orientation state; these play an important role in determining the mechanical properties. Although the PP films with EVMT had lower crystallinity, they also had higher tensile strengths, Young moduli, yield stresses, and stresses at break than pure PP, with the exception of the elongation at break (Table VII).

The improved mechanical properties manifested as a 4–12% rise in the tensile strength, a 4–14% rise in Young's modulus and yield stress, and a 28–158% rise in the stress at break for PP with added percentages (0.1–2.0%) of EVMT. These were attributed to EVMT's orientation effect during the film-blowing process, even though EVMT decreased the PP crystallinity. For a semicrystalline polymer with a small or large crystal grain size, at the same volume fraction of crystallinity, the polymer with the small crystal grain size appeared to have a lower $\Delta H_c$ than that that with the large crystal grain size because a crystal with a small grain size had more surface area and a larger amount of crystal defects. The platelike particles of EVMT, arranged in parallel in the PP films, limited the PP crystal grain diameter; this was smaller than the space between the two neighboring plates of EVMT. In most cases, this resulted in a decrease in $\Delta H_c$.

The PP chains were adsorbed on platelike particles in the EVMT–PVOH–PP nanocomposites. The platelike particles acted as physical cross-points, enhancing the intermolecular forces between the PP chains and reducing the crystal grain size. This results in strength and toughness for PP with 0.1% EVMT, whose elongation at break increased by 25% compared with that of pure PP film. However, for PP with 0.3% EVMT or greater, the elongation at break began to decrease. When more EVMT was added to the PP, the number of PP chains between the two plates was so small that the probability of the PP chain entanglement was reduced, and the elongation at break decreased. In particular for PP with 2% EVMT, the PP chains packaged platelike particles, and this caused whole movement of platelike particles with PP chains. At the moment, the stretch-oriented degree of the PP chains was already large during the blowing process, so brittle fracture happened easily during the stress–strain measurement. Rigid EVMT particles increased the modulus of the modified PP films. The modulus value increased with the addition of EVMT, mainly because of the strong interactions between the PP matrix and EVMT–PVOH via van der Waals forces.

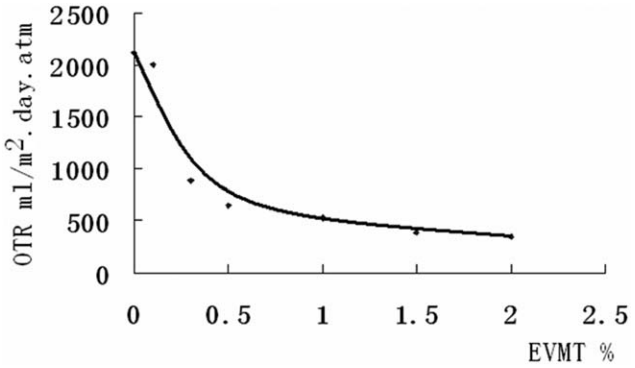


**Figure 6.** Effects of various amounts of EVMT on the OTR of PP films.

### Gas Barrier Model with Platelike Particles of EVMT

The platelike particles of EVMT in the PP films resulted in sharply decreasing OTRs (Figure 6). The OTR through the PP film containing 2.0% platelike particles was 84% lower than that through the pure PP film; this could be explained by solution–diffusion theory. According to this theory, gas permeation through a film is generally described as a solution–diffusion process:

$$K = DS \quad (1)$$

where $K$ is the gas permeability coefficient, $D$ is the diffusion coefficient, and $S$ is the gas solubility coefficient.

**Table VII.** Mechanical Properties of the PP Films with and without EVMT Filling

| PP sample | EVMT (%) | Tensile strength (MPa) | Young's modulus (MPa) | Yield stress (MPa) | Stress at break (MPa) | Elongation at break (%) |
|---|---|---|---|---|---|---|
| 1 | 0.0 | 36.3 ± 1.2 | 1090 ± 43 | 30.5 ± 1.4 | 15.0 ± 1.1 | 75.8 ± 7.4 |
| 2 | 0.1 | 38.8 ± 1.8 | 1150 ± 51 | 32.5 ± 1.5 | 19.2 ± 2.0 | 94.8 ± 8.3 |
| 3 | 0.3 | 39.0 ± 0.9 | 1180 ± 53 | 32.2 ± 1.2 | 19.5 ± 2.0 | 24.4 ± 2.0 |
| 4 | 0.5 | 37.9 ± 1.2 | 1140 ± 41 | 31.8 ± 1.4 | 35.3 ± 3.1 | 8.74 ± 1.0 |
| 5 | 1.0 | 39.8 ± 1.6 | 1200 ± 44 | 32.7 ± 1.1 | 35.6 ± 2.4 | 15.5 ± 1.4 |
| 6 | 1.5 | 38.4 ± 1.7 | 1210 ± 55 | 31.3 ± 1.3 | 35.4 ± 3.5 | 11.7 ± 1.2 |
| 7 | 2.0 | 40.7 ± 0.6 | 1250 ± 20 | 34.7 ± 0.4 | 38.7 ± 1.0 | 7.41 ± 0.1 |

The platelike particles of EVMT could simultaneously decrease $D$ and $S$. As described earlier, the platelike particles of EVMT arranged in parallel in the PP films decreased the PP crystal grain diameter. A larger number and smaller size of crystallites in the PP films containing platelike particles shortened the distance between the crystalline regions and, therefore, also shortened the chain length in the amorphous regions; this caused a reduction in the PP chain mobility. The platelike structure of EVMT provided a large surface area and, therefore, a large EVMT–PP intermolecular interaction.[24] The presence of the platelike particles themselves also restrained the mobility of the PP chains surrounding the platelike particles; in particular, if nucleation occurred, winch was affirmed through a comparison $\Delta H_c$ of samples 1 and 2 in the DSC data in Table IV. A reduction in the chain mobility in the amorphous parts of the polymer chains due to the presence of nanoparticles[25–27] led to an increase in the glass-transition temperature and a decreased fraction of the films' free volume; this caused a decreasing $S$ in the films.

Additionally, parallel-arranged platelike particles of EVMT in the PP films increased the diffusion path length, and this led to a loss in the diffusivity, that is, the nanoparticles acted as obstacles. As a result, the enhancement of the barrier properties depended not only on the volume fraction of nanoparticles present in the PP matrix but also on the shape (aspect ratio) of the nanoparticles. This took into account in Nielsen's model, which describes the effect of platelike particles on the gas permeability in polymers:[28]

$$\frac{K_{\text{composite}}}{K_{\text{matrix}}} = \frac{1-\phi}{1+\frac{\alpha}{2}\phi} \tag{2}$$

where $\varphi$ is the volume fraction of platelike particles and $\alpha$ is the aspect ratio (length divided by width) of the individual filler particles, and "$K_{\text{composite}}$" and "$K_{\text{matrix}}$" are the gas permeability coefficient value of the PP–nanoparticle composite film and pure PP matrix respectively.

When the content of platelike particles of EVMT in PP was 0.1–2.0%, the OTR of the modified PP decreased with increasing content of EVMT (Figure 6). According to this fitting OTR curve, good agreement with this model was found for the oxygen permeability in the PP films filled with EVMT nanoparticles. The fitting curve proved that the aspect ratio equaled 550. This verified achievement included the intercalation and exfoliation of EVMT in the PVOH–water solution with the ball-milling process, through which platelike particles with a high aspect ratio were obtained. The improved barrier properties were contributed mainly by the EVMT nanoparticles rather than PVOH, which was not in crystalline form in the modified films. As shown in the XRD spectra in Figure 1, characteristic diffraction peaks with PVOH were not exhibited by the PVOH–EVMT (95:5) nanocomposite; moreover, they were not seen in the PVOH–EVMT–PP blend films that contained 2% PVOH or less.

## CONCLUSIONS

The mechanical ball-milling of EVMT in the PVOH–water solution made it possible to form an EVMT–PVOH nanocomposite in which PVOH macromolecules intercalated into the interlayer space of EVMT, and the EVMT was exfoliated to platelike particles. By melt-blending with PP, EVMT was sheared and further exfoliated into nanoparticles with a high aspect ratio (ca. 550). Compared with the unmodified PP, when the EVMT nanoparticle loading was 0.1%, the strength and toughness of the modified film improved. For modified PP films with 0.3% or more EVMT, the tensile strength, modulus, yield stress, and stress at break all increased, with the exception of the elongation at break. The rigid EVMT particles increased the thermal stability and gas barrier properties of the modified PP films.

These improved properties were caused by an optimal microstructure: (1) PVOH serves well as a compatibilizer between EVMT nanoparticles and the PP matrix; (2) the EVMT platelike particles were packaged by polar PVOH; (3) the EVMT played a role as a heterogeneous nucleation agent and physical crosslinking point, increasing PP's crystallization ability and cohesive energy; (4) the parallel arrangement of EVMT particles was caused by the stretching orientation in the film-blowing process; (5) parallel-arranged EVMT had a high aspect ratio (ca. 550); and (6) the PP crystal diameter was less than the distance between two neighboring parallel-arranged platelike particles of EVMT.

## ACKNOWLEDGMENTS

This work was financially supported by the National Natural Science Foundation of China (contract grant number 31471653) and the Science and Technology Committee Project of the Beijing Institute of Graphic Communication.

## REFERENCES

1. Martin, R. T.; Bailey, S. W.; Eberl, D. D.; Fanning, D. S.; Guggenheim, S.; Kodama, H.; Pevear, D. R.; Srodon, J.; Wicks, F. J. *Clays Clay Miner.* **1991**, *39*, 333.
2. Zhang, K.; Xu, J.; Wang, K. Y.; Cheng, L.; Wang, J.; Liu, B. *Polym. Degrad. Stab.* **2009**, *94*, 2121.
3. Osman, M. A. *J. Mater. Chem.* **2006**, *16*, 3007.
4. Martynková, G. S.; Valášková, M.; Capková, P.; Matejka, V. *J. Colloid Interface Sci.* **2007**, *313*, 281.
5. Jiřímališ, M. K. *Acta Geodyn. Geomater.* **2005**, *2*, 105.
6. Tjong, S. C.; Meng, Y. Z.; Xu, Y. *J. Appl. Polym. Sci.* **2006**, *86*, 2330.
7. Li, D.; Xu, W.; Qi, Y.; Shang, W.; Fu, Y.; Liao, R. *Polym. Compos.* **2015**, *36*, 78.
8. Fu, Y.; Li, D.; Xu, W.; Qi, Y.; Shang, W.; Wu, W.; Wang, Y. *J. Appl. Polym. Sci.* **2014**, *131*, 40954.
9. Mandelkern, L.; Alamo, R. G. In Physical Properties of Polymers Handbook; Mark, J. E., Ed.; American Institute of Physics: New York, **1996**.
10. Marta, V.; Grazyna, S. M., eds.; Clay Minerals in Nature-Their Characterization, Modification and Application; InTech, **2012**; Chapter 11.
11. Walker, G. F. *Clays Clay Miner.* **1956**, *4*, 101.

12. Walker, G. F. Vermiculites Minerals. In: The X-Ray Identification and Crystal Structure of Clay Minerals; Brown, G., Ed.; Mineralogical Society: London, **1961**; p 297.
13. Marcos, C.; Argüelles, A.; Ruíz-Conde, A.; Sánchez-Soto, P. J.; Blanco, J. A. *Miner. Mag.* **2003**, *67*, 1253.
14. Marcos, C.; Arango, Y. C.; Rodriguez, I. *Appl. Clay Sci.* **2009**, *42*, 368.
15. Huo, X.; Wu, L.; Liao, L.; Xia, Z.; Wang, L. *Powder Technol.* **2012**, *224*, 241.
16. Majdzadeh-Ardakani, K.; Nazari, B. *Compos. Sci. Technol.* **2010**, *70*,1557.
17. Tee, T.-T.; Sin, L. T.; Gobinath, R.; Bee, S.-T.; Hui, D.; Rahmat, A. R.; Kong, I.; Fang, Q. *Compos. B* **2014**, *47*, 238.
18. Tai, L. M. *Adv. Mater. Res.* **2011**, *399*, 1257.
19. Jang, J.; Lee, D. K. *Polymer* **2004**, *45*, 1599.
20. Marcinčin, A.; Jurčišinová, Z.; Borsig, E.; Krištofič, M.; Marcinčinová, T. *Polym. Adv. Technol.* **2001**, *12*, 461.
21. Merkel, T. C.; Freeman, B. D.; Spontak, R. J.; He, Z.; Pinnau, I.; Meakin, P.; Hill, A. J. *Ultrapermeable Sci.* **2002**, *296*, 519.
22. Winberg, P.; Desitter, K.; Dotremont, C.; Mullens, S.; Vankelecom, I. F. J.; Maurer, F. H. J. *Macromolecules* **2005**, *38*, 3776.
23. Valášková, M.; Martynková, G. S.; Matějka, V.; Barabaszová, K.; Plevová, E.; Měřínská, D. *Appl. Clay Sci.* **2009**, *43*, 108.
24. Okhamafe, A. O.; York, P. *Int. J. Pharm.* **1984**, *22*, 265.
25. Kersch, M.; Fabris, F. W.; Stumpf, M.; Richter, F.; Schmidt, H.-W.; Altstädt, V. J. *Plast. Technol.* **2012**, *8*, 331.
26. Xu, B.; Zheng, Q.; Song, Y.; Shangguan, Y. *Polymer* **2006**, *47*, 2904.
27. Alexandre, B.; Colasse, L.; Langevin, D.; Médéric, P.; Aubry, T.; Chappey, C.; Marais, S. *J. Phys. Chem. B* **2010**, *114*, 8827.
28. Nielsen, L. E. J. *Macromol. Sci. Chem.* **1967**, *1*, 929.